Lattice dynamical probe of phase transformations in niobium oxyfluoride Nb_{2}O_{2}F_{3}

Alexander P. Litvinchuk, Melissa Gooch, Bernd Lorenz, Clarina R. de la Cruz, George N. Oh, and Arnold M. Guloy

Phys. Rev. B **97**, 094306 — Published 28 March 2018

DOI: 10.1103/PhysRevB.97.094306

Lattice dynamical probe of phase transformations in niobium oxyfluoride $Nb_2O_2F_3$

Alexander P. Litvinchuk, Melissa Goosh, and Bernd Lorenz
Texas Center for Superconductivity and Department of Physics, University of Houston, Houston, Texas 77204-5002, USA

Clarina R. de la Cruz
Quantum Condensed Matter Division, Oak Ridge National Laboratories, Oak Ridge, Tennessee 37831, USA

George N. Oh and Arnold M. Guloy
Texas Center for Superconductivity and Department of Chemistry, University of Houston, Houston, Texas 77204-5003, USA

Raman scattering spectroscopy is used to monitor the transition of reduced niobium oxyfluoride $Nb_2O_2F_3$ single crystals from their high-temperature monoclinic (*I2/a*) into the low-temperature triclinic ($P\overline{1}$) phase at $T_c \approx 90$ *K* due to charge disproportionation of $(Nb\text{-}Nb)^{7+}$ dimers and creation of crystallographically non-equivalent dimers with a long and a short Nb-Nb bonds. The group theoretical analysis of lattice vibrations is performed and the assignment of observed phonon lines to the specific lattice eigenmodes of the two phases is achieved based on a comparison with the results of density functional lattice dynamics calculations. Nb-Nb dimers are found to possess stretching vibrational frequencies as high as 382 cm^{-1}. Strikingly, the kinetics of the monoclinic-to-triclinic structural transformation and the volume fraction of corresponding phases below T_c is shown to strongly depend upon the sample cooling rate. Fast cooling results in a "freezing" of the high-temperature monoclinic phase and allows to observe a spin-ordered state below $T_N \approx 49$ K.

PACS numbers: 63.20.D-, 78.30.Er, 64.70.kp

I. INTRODUCTION

Recent interest toward reduced niobium (III/IV) oxyfluoride crystals, $Nb_2O_2F_3$, is due to their unique chemical and physical properties and a delicate interplay between charge, spin, and orbital degrees of freedom, despite apparent structural similarity to the well known Nb_2O_5 compound[1]. In this sense the $Nb_2O_2F_3$ became a model material for uncovering a non-trivial relationship between chemical bonding and magnetism in 3*d*, 4*d* and 5*d* transition metals compounds.[2–5] Interestingly, Nb ions are strongly bonded in $Nb_2O_2F_3$ with one unpaired electron per $(Nb\text{-}Nb)^{7+}$ dimer in the high-temperature phase. Upon cooling $Nb_2O_2F_3$ exhibits two phase transitions, which have previously been identified by X-ray diffraction, magnetic, and heat capacity measurements.[1] Below 90 K, a first order structural transition takes place, which is accompanied by the charge disproportionation between distinct Nb-Nb dimers. At lower temperature (near 49 K), a sharp peak of the heat capacity and an anomaly of the magnetic susceptibility indicate another transition, the nature of which is not yet fully understood.

Despite of initial structural, magnetic, and thermodynamic studies, the vibrational properties of $Nb_2O_2F_3$ remain unexplored. Of special interest here, apart from the assignment of observed phonon lines, is also a long standing issue of the interpretation of spectra of metal cluster compounds, and in particular the effect of metal-metal bonding on their vibrational spectra.[6–8]

In this paper we report on an experimental Raman scattering spectroscopic study of vibrational modes of both the high-temperature monoclinic phase of $Nb_2O_2F_3$ and its low-temperature triclinic modification. The assignment of observed vibrational modes to the specific lattice eigenmodes is based on a close comparison with the results of density functional theory (DFT) lattice dynamics calculations. Further, Raman spectroscopy is used to monitor the dynamics of the structural phase transition. Strikingly, a pronounced kinetics of this transition is detected, such that the transition could be clearly observed to occur during extended time interval of up to 30-60 minutes. On the other hand, it is shown that the high-temperature monoclinic phase could be "frozen" upon fast cooling of $Nb_2O_2F_3$ to low temperatures.

II. SAMPLES, EXPERIMENTAL AND CALCULATION TECHNIQUES

$Nb_2O_2F_3$ crystals were synthesized from the reaction of Nb, SnF_2, and SnO in Sn flux within welded Nb containers, enclosed in evacuated fused silica jackets, as reported earlier in Ref. 1. The typical size of crystals was about 50×30×150 μm. X-ray powder diffraction as well as single crystal diffraction experiments revealed unambiguously the monoclinic structure of $Nb_2O_2F_3$ at room temperature: space group *I2/a* (no. 15), lattice parameters $a = 5.7048(1)\AA$, $b = 5.1610(1)\AA$, $c = 12.2285(2)\AA$, $\beta = 95.751(1)^\circ$, unit cell volume $V = 358.225(11)\AA^3$. The structure of the low-temperature phase (below $T_c =$ 90 K) was found to be triclinic: space group $P\overline{1}$ (no. 2), lattice parameters $a = 5.1791(5)\AA$, $b = 5.7043(6)\AA$, $c = 6.8911(7)\AA$, $\alpha = 108.669(3)^\circ$, $\beta = 109.922(2)^\circ$, $\gamma =$

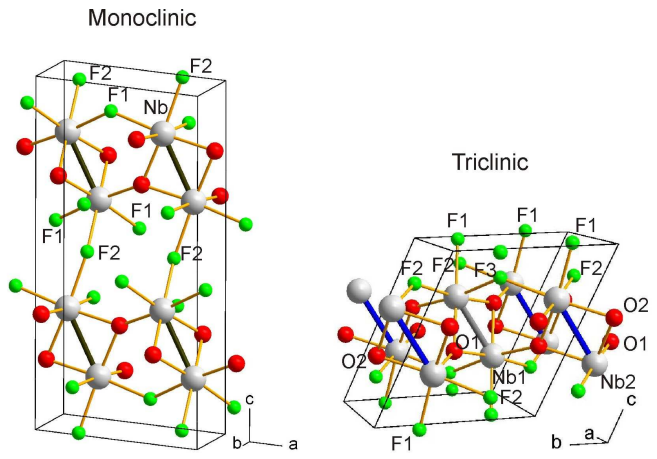

FIG. 1: (Color online) Crystal structure of the high-temperature monoclinic and the low-temperature triclinic phases of $Nb_2O_2F_3$. Nb-Nb dimers are crystallographically equivalent within the monoclinic phase (Nb-Nb bonds are shown by thick black lines), but due to the charge disproportionation are non-equivalent in the low-temperature phase. The short Nb1-Nb1 bond is depicted in gray, while the long (Nb2-Nb2) bonds - in blue. Oxygen atoms are shown in red, F - in green, Nb in grey.

$90.332(3)^\circ$, V = $179.82(3)\mathring{A}^3$.

Crystallographic structure of both high-temperature monoclinic and low-temperature triclinic phases of $Nb_2O_2F_3$ are shown in Fig. 1. The unit cell of the monoclinic phase is centered so that its primitive cell contains only half of the unit cell volume (2 formula units, or 14 atoms in the primitive cell). It features two equivalent Nb-Nb dimers with rather short $2.5739(1)\mathring{A}$ bond length. The dimers are connected via oxygen and fluorine vertices to form the three dimensional structure.

Unlike the high-temperature monoclinic phase, the unit cell of the triclinic phase contains two non-equivalent Nb-Nb dimers: one doubly bonded with the short bond $(2.5000(9)\mathring{A})$ and one singly bonded with a longer bond $2.6560(9)\mathring{A}$. Formation of these dimers is a consequence of the charge disproportionation.[1,2]

Raman scattering spectra were excited with the 514.5 nm line of an Ar^+ ion laser and recorded in the back-scattering geometry with a Horiba Jobin Yvon 64000 triple spectrometer equipped with an optical microscope and a liquid nitrogen cooled CCD detector. The spectral resolution was 1.5 cm^{-1}. Laser power within the excitation spot of about 2 μm in diameter was kept below 2 mW in order to minimize heating of the sample. By comparing current temperature dependent Raman scattering data with earlier reported heat capacity measurements[1] we estimated that heating within the laser excitation spot does not exceed 4 K. Variable temperature measurements were performed with a helium flow Oxford Microstat, where the sample temperature was controlled within 0.1 K.

The first principle calculations of the electronic ground state of both structural modifications of $Nb_2O_2F_3$ were performed within the generalized gradient approximation using the Perdew-Burke-Ernzerhof local functional[9] as implemented in the CASTEP code.[10] Norm-conserving pseudopotentials were used. Prior to performing calculations the structures were relaxed while keeping lattice parameters fixed and equal to the experimentally determined ones, so that forces on atoms in the equilibrium position did not exceed 10 meV/Å. For calculations of the electronic structure and other relevant electronic properties an integration within the Brillouin zone was performed over a 5×5×4 Monkhorst-Pack grid[11] in reciprocal space. The plane wave basis cut-off was set to 850 eV. Lattice dynamics properties were further accessed via finite displacement method on a 2×2×1 supercell.

III. RESULTS AND DISCUSSION

A. DFT lattice dynamics calculations and the phonon modes assignment

First of all, it is instructive to perform a group theoretical analysis[12] of vibrational spectra of both phases of $Nb_2O_2F_3$ in order to determine the number and symmetry of modes, which are expected to contribute to Raman scattering spectra. In Tables I and II the results of such analysis are summarized.

TABLE I: Wyckoff position, site symmetry, and irreducible representations of atoms within the high-temperature monoclinic phase of $Nb_2O_2F_3$ (space group *I2/a*).

Atom	Wyckoff notation	Site symmetry	Irreducible representantions
Nb	8f	C_1	$3A_g + 3A_u + 3B_g + 3B_u$
F1	8f	C_1	$3A_g + 3A_u + 3B_g + 3B_u$
F2	4e	C_2	$A_g + A_u + 2B_g + 2B_u$
O	8f	C_1	$3A_g + 3A_u + 3B_g + 3B_u$

Mode classification

$\Gamma_{\text{acoustic}} = A_u + 2B_u$

$\Gamma_{\text{Raman}} = 10A_g + 11B_g$

$\Gamma_{\text{IR}} = 9A_u + 9B_u$

We note that the primitive cell of both phases contains the same amount of atoms (14) so that the total number of optical vibrational modes remains the same for both structural modifications of $Nb_2O_2F_3$. F2 atoms of the high temperature monoclinic phase occupy crystallographic sites with the C_2 symmetry, while all others - general position sites with the C_1 symmetry. Thus, following Table I, one expects 21 $(10A_g + 11B_g)$ Raman active modes for this phase. On the other hand, all atoms of the low-temperature triclinic phase occupy general position sites and generate the same amount of Raman-active modes ($21A_g$).

TABLE II: Wyckoff position, site symmetry, and irreducible representations of atoms within the low-temperature triclinic phase of $Nb_2O_2F_3$ (space group $P\bar{1}$).

Atom	Wyckoff notation	Site symmetry	Irreducible representantions
Nb1	2i	C_1	$3A_g + 3A_u$
Nb2	2i	C_1	$3A_g + 3A_u$
F1	2i	C_1	$3A_g + 3A_u$
F2	2i	C_1	$3A_g + 3A_u$
F3	2i	C_1	$3A_g + 3A_u$
O1	2i	C_1	$3A_g + 3A_u$
O2	2i	C_1	$3A_g + 3A_u$

Mode classification

$\Gamma_{\text{acoustic}} = 3A_u$

$\Gamma_{\text{Raman}} = 21A_g$

$\Gamma_{\text{IR}} = 18A_u$

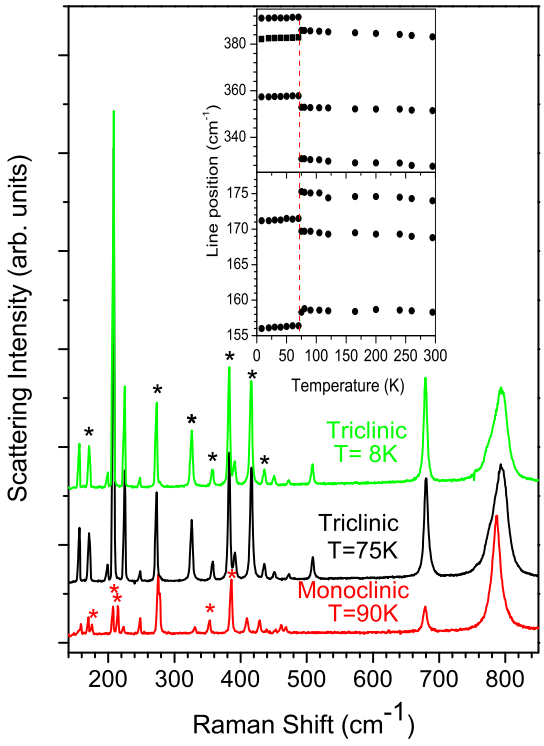

FIG. 2: (Color online) Raman scattering spectra of the high-temperature monoclinic (red line, T=90 K) and the low-temperature triclinic (T=75 K and 8 K) phases of $Nb_2O_2F_3$. Asterisks mark the lines which, according to the DFT calculations, involve Nb motion. The insert shows the temperature-dependent position of selected lines. Dashed vertical line marks the structural transition temperature T_c.

In Fig. 2 experimental Raman spectra of $Nb_2O_2F_3$ in its monoclinic (T = 90 K) and triclinic (T = 75 K and 8 K) modifications are presented, which are both characterized by a series of narrow intense lines, proving a good quality of crystal under investigation. The total number of lines in both spectra remains the same. Between the room temperature and about 90 K (in the monoclinic phase) the lines exhibit some frequency hardening and line width narrowing due to lattice anharmonicity. At the structural transition temperature $T_c \approx 90\ K$, however, one observes an abrupt shift of the lines by as much as 8 cm^{-1} and redistribution of their relative intensities. Importantly, there is no evidence of any additional structural phase transition upon further lowering the temperature down to 8 K. At the same time one can notice an anomalous softening of mode frequencies below T_c from the data presented in the insert of Fig. 2, which will be analyzed in more detail later on.

The assignment of observed phonon lines to the specific lattice eigenmodes is performed based on a comparison of experimental mode frequencies with the results of DFT lattice dynamics calculations. Moreover, the analysis of relative intensities of spectral lines of monoclinic $Nb_2O_2F_3$ under parallel and crossed polarizations of excitation laser and scattered beams allowed us to distinguish A_g (which are expected to be stronger in the parallel scattering polarization) and B_g symmetry modes. It turns out that they coincide very well with the symmetries, predicted by calculations and summarized in Table III.

We have to note that calculations produced several modes with slightly negative frequencies, so that calculated results for the low-frequency modes should be considered with caution. However, as it is seen from Table III, for the modes in the frequency interval of interest (above 165 cm^{-1}) there seems to be a reasonable agreement between calculated and experimental data (the mean deviation of experimental frequencies from calculated ones is only 3.2%), which justifies presented comparative analysis.

The analysis of mode vibrational patterns clearly shows that there is a number of modes, which involve Nb motion. They are marked with an asterisk in experimental spectra of Fig. 2 and are shown in bold face in Table III. The importance of identifying those mode steams from the fact that "bonded" metal atoms are likely to generate higher frequency stretching vibrations compared to "unbonded" ones. Despite general complexity of mode vibrational patterns such that several atoms are simultaneously involved in a given vibration, in the case of $Nb_2O_2F_3$ both theory and experiment point toward the existence of Nb-Nb stretching modes with frequencies as high as 382 cm^{-1} despite rather high atomic weight of Nb (92.9 at. units). Vibrational modes of Nb with frequencies up to 300 cm^{-1} were earlier observed in the cubic symmetry cluster compound Nb_6F_{15}, which features Nb_6 octahedra as the central building block of the structure.[6]

TABLE III: Experimental and DFT-calculated Raman-active vibration frequencies of the high-temperature monoclinic and the low-temperature triclinic phases of $Nb_2O_2F_3$. The frequencies shown in bold correspond to the modes involving Nb motion. Note that Nb1-Nb1 and Nb2-Nb2 refer to the short and long dimers in the triclinic phase. All data are in cm^{-1}.

Monoclinic phase			Triclinic phase		
Exper.	Theory (symmetry)	Main displacements	Exper.	Theory (mode symmetry)	Main displacements
169					
175	**167** (B_g)	tilt Nb-Nb	**171**	**166** (A_g)	stretch-tilt Nb1-Nb1
206	**201** (A_g)	tilt-stretch Nb-Nb	198		
213	**207** (B_g)	tilt Nb-Nb	207	213 (A_g)	O1 rotation about Nb1-Nb1
223			224		
247	245 (A_g)	F2	247		
276	280 (B_g)	O	**272**	**275** (A_g)	tilt Nb1-Nb1 + O1
331	311 (A_g)	F1 + F2	**326**	**334** (A_g)	stretch Nb1-Nb1 + F2 + O1
353	**339** (B_g)	stretch-tilt Nb-Nb +F2	**357**	**363** (A_g)	stretch-tilt Nb2-Nb2 + F1
385	**405** (A_g)	tilt Nb-Nb + F2	**382**	**364** (A_g)	stretch-tilt Nb1-Nb1 + F3
410	426 (B_g)	F2 + F1 + O	**416**	**410** (A_g)	tilt Nb1-Nb1 + O1 +F3
429			**434**	**422** (A_g)	tilt Nb1-Nb1 + tilt Nb2-Nb2 + O1
452	451 (A_g)	O	449		
468	472 (B_g)	F2	473	456 (A_g)	F2
	504 (A_g)	F2+F1	508	484 (A_g)	O2
678	750 (B_g)	out-of-phase O around Nb-Nb	678	743 (A_g)	O2 around Nb2-Nb2
786	788 (A_g)	in-phase O around Nb-Nb	795	803 (A_g)	O1 around Nb1-Nb1

Remarkably, the modes involving Nb atoms appear to be the most intense in the Raman scattering spectra, a fact which was earlier documented in Ref. 6. Obviously, it is a consequence of high polarizability of corresponding vibrations. As an example, vibrational modes calculated at 275 and 364 cm^{-1} and representing two intense lines of the low-temperature triclinic phase, are shown in Fig. 3. The first one involves tilting of the Nb1-Nb1 dimer along with deformation of $Nb1_2$-$O1_2$ structural unit. The other mode is due to stretch-tilt of Nb1-Nb1 dimer with simultaneous modulation of Nb1-F3 bonds.

As far as higher frequency oxygen related vibrations, Fig. 4 shows Raman scattering spectra of both phases

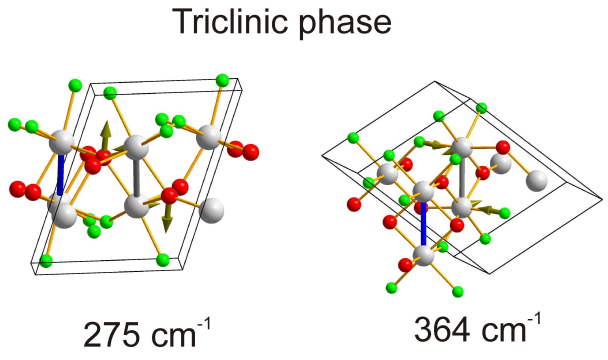

FIG. 3: (Color online) Vibrational pattern of the two modes in the low-temperature triclinic phase of $Nb_2O_2F_3$, calculated at 275 and 364 cm^{-1}.

of $Nb_2O_2F_3$ along with the vibrational patterns of corresponding modes. According to the DFT lattice dynamics calculations, for both phases there exist only two Raman-active modes in the frequency range above 510 cm^{-1}. In the case of monoclinic high-temperature phase, they correspond to the in-phase (calculated at 788 cm^{-1}) and at lower frequency out-of-phase motion of oxygen around Nb-Nb dimers, as shown by the lower panel pictures in Fig. 4. For the low-temperature triclinic phase one expects, instead, the mode due to fully symmetric oxygen motion around the short Nb1-Nb1 dimer (calculated to be at 803 cm^{-1}, somewhat higher with respect to the mode in the monoclinic phase) along with lower lying line with oxygen motion around the long Nb2-Nb2 dimer.

Of principal importance is a complex line shape of the highest frequency band in the low-temperature triclinic phase of $Nb_2O_2F_3$, shown in the right upper corner of Fig. 4. It is obviously a superposition of two closely lying lines. The lower-frequency component practically coincides in the position with the line of the monoclinic high-temperature phase, while the higher frequency component corresponds apparently to the "intrinsic" triclinic phase vibration. This fact points toward apparent coexistence of the two phases of $Nb_2O_2F_3$ at sample temperatures below the T_c, as determined from crystallography experiments. As we will see further on, this is indeed the case.

As already mentioned, an anomalous softening of mode frequencies upon cooling below T_c (triclinic phase) is observed. Indeed, the well established model for anharmonic phonon decay through phonon-phonon scat-

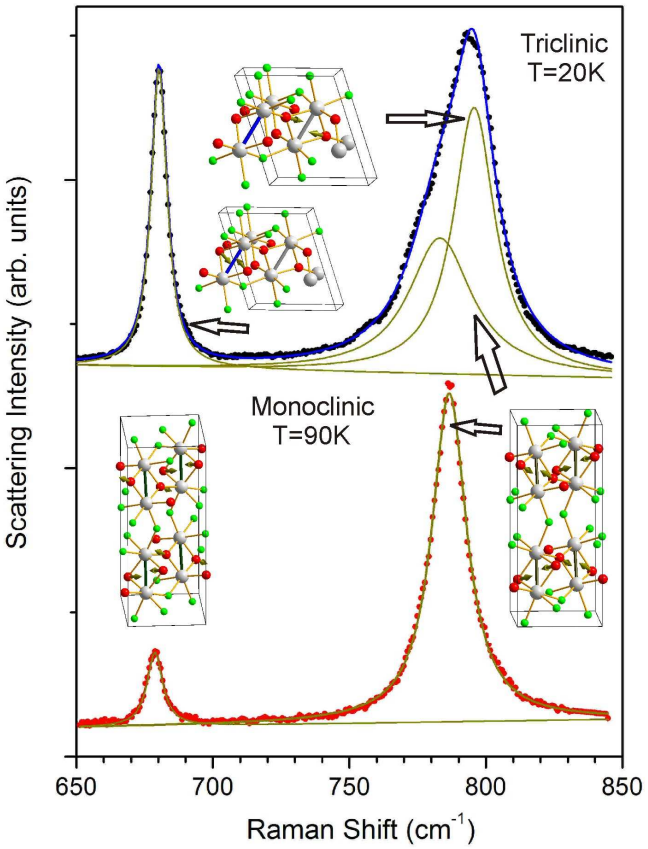

FIG. 4: (Color online) High-frequency part of Raman spectra of $Nb_2O_2F_3$: lower frame - monoclinic phase, upper frame - triclinic phase. Points - experimental data, solid lines - results of fitting to Lorentzian profiles. DFT-calculated vibrational patterns of corresponding modes are shown next to each line. Rather large width and complex line shape of the highest frequency mode for the low temperature spectrum (upper right corner), that signal coexistence of two phases, is obvious.

tering describes temperature dependencies of the mode frequency (ω) and the line width (Γ) for crystals as follows[13,14]:

$$\omega(T) = \omega_0 - \frac{2A}{e^{h\omega/2k_BT} - 1},$$

$$\Gamma(T) = \Gamma_0 + \frac{2B}{e^{h\omega/2k_BT} - 1},$$

(were ω_0 and Γ_0 are mode frequency and line width at T=0 K, $h\omega$ is the phonon energy, and k_B is Boltzmann constant, while A and B are positive constants), thus predicting hardening of mode frequency and narrowing of line width upon lowering temperature. It is opposite to what is experimentally observed for Raman-active modes of $Nb_2O_2F_3$ below T_c. Note that modes shown in Fig. 5 represent not only modes that involve Nb displacements (with frequencies around 171 and 382 cm^{-1}), but

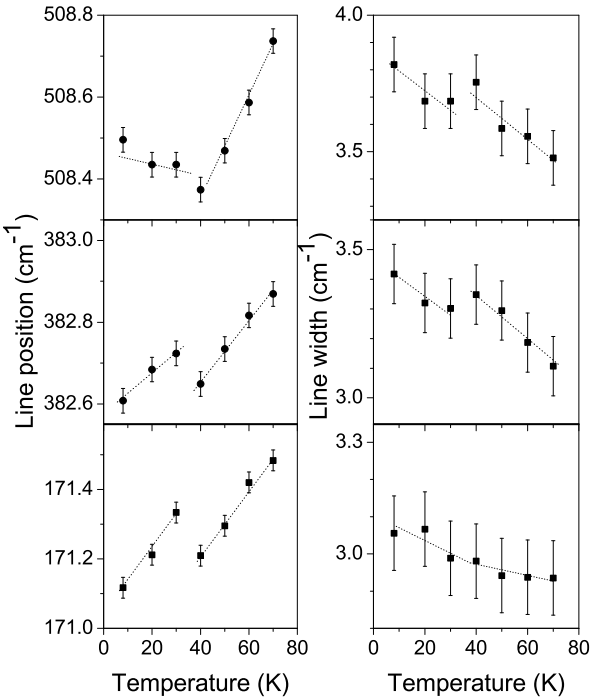

FIG. 5: Temperature dependence of phonon parameters of $Nb_2O_2F_3$ in the triclinic phase. Dotted lines are guide for the eye.

also the one where O2 motion dominates (at 508 cm^{-1}). Other Raman modes $Nb_2O_2F_3$ show qualitatively similar temperature behavior. Quantitatively, observed anomalies are rather weak (0.2 - 0.4 cm^{-1} for both frequency and line width) in comparison with those reported earlier for rare earth manganese oxides[15,16] and other magnetic materials[17].

It is plausible to expect that observed anomalous behavior in the low-temperature triclinic phase of $Nb_2O_2F_3$ could be due to phonon coupling to underlying magnetic excitations. The results of magnetic measurements, however, indicate the absence of a global long range magnetic state of triclinic $Nb_2O_2F_3$ at low temperatures. Thus, the anomalies could be associated with either fluctuations of magnetization or a presence of microscopic domains of magnetic monoclinic phase. We also want to point out that both mode frequency and line width exhibit some kind of discontinuity around 40 K, which might signal modification of magnetic structure of $Nb_2O_2F_3$. As revealed by magnetic measurements, such changes indeed takes place and will be discussed in the Section III B.

It is also worth noting that spectra of $Nb_2O_2F_3$ exhibit rich multi-phonon structure, typical of ionic materials, II-VI semiconductors for example. For the zinc-blend based binary tetrahedrally coordinated semiconducting compounds there is only one optical vibrational mode, the longitudinal (LO) component of which typically shows a series of intense multi-phonon overtones

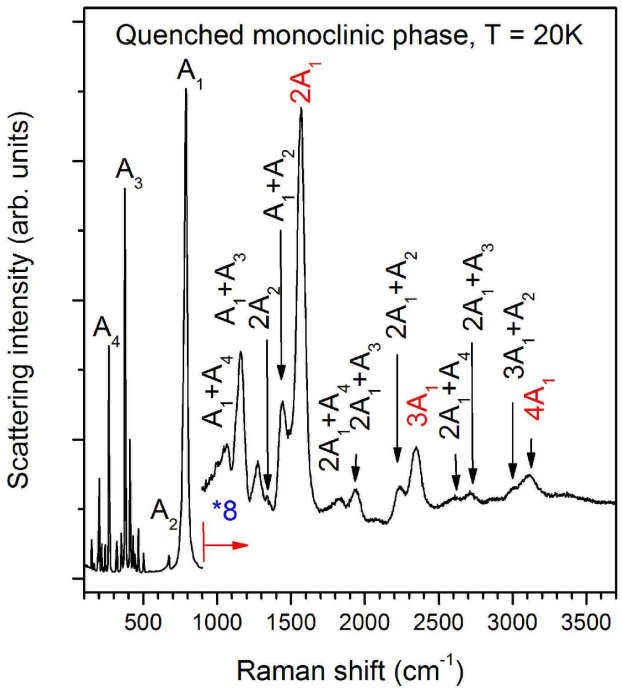

FIG. 6: (Color online) Multi-phonon Raman scattering spectrum of quenched monoclinic $Nb_2O_2F_3$ taken at T = 20 K. Note an enlarged by factor of 8 high-frequency part of the spectrum.

under resonant excitation.[18,19] This is the consequence of the Fröhlich-interaction-induced electron-LO-phonon coupling. Similar effects have been documented for materials with several LO-modes (alloys of binary compounds and ternary semiconducting materials), which showed an enhanced role of combinational lines with respect to the overtones.[20,21] Recently intense multi-phonon processes (overtones of LO-modes as well as combinations of LO phonons with non-polar fully symmetric A_g modes) have been reported for the quaternary semiconductor $Cu_2Zn(Ge,Sn)S_4$.[22]

In the case of $Nb_2O_2F_3$, as it was shown above, all Raman-active phonons are non-polar so that they do not possess any LO-TO splitting. Despite of this, as it is seen in Fig. 6, one clearly observes overtones of the most intense line A_1 (at 788 cm^{-1}) up to the forth order. Many lines involving combinations of other intense Brillouin zone-center lines (those at 678, 382, and 282 cm^{-1}, which are marked in Fig. 6 as A_2, A_3, and A_4, respectively) are also observed in the multi-phonon spectrum. It is worth mentioning that, if one compares relative intensities of combinational lines $(n-1)A_1 + A_2$ with respect to overtones nA_1 of the same order, obvious is a rise of relative intensity of the former as the scattering order (n) increases. It is the consequence of an increase of the number of possible diagrams for the multi-phonon scattering processes, like in the case of earlier studied materials with several non-equivalent LO phonons.[20,21]

B. Kinetics of the monoclinic-to-triclinic phase transition: Raman scattering and magnetization

As we already mentioned, the analysis of the Raman scattering line shapes of high frequency oxygen-related modes (shown in Fig. 4) indicated a non-trivial relation between volume fraction of monoclinic and triclinic phases and points toward their possible coexistence. It turns out that sample cooling rate and a pre-history of warming-cooling is of prime importance for the observed relative volume fraction of monoclinic and triclinic phases in the crystal. In particular, our magnetic measurements revealed the appearance of a spin-order phase below about 49 K, volume fraction of which depends on the sample cooling rate in a way that faster cooling results in a higher volume fraction of spin-ordered monoclinic phase.[1]

As an example of a non-trivial kinetics of the monoclinic-to-triclinic phase transition, we show in Fig. 7 the results of the following experiment: from initial sample temperature of 100 K (the monoclinic phase) the sample was cooled down to the temperature of 78 K (slightly below T_c) and the temperature was kept constant. A series of spectra were taken with several minutes interval in order to monitor the development of the triclinic phase. In the selected spectral interval 404-422 cm^{-1} one

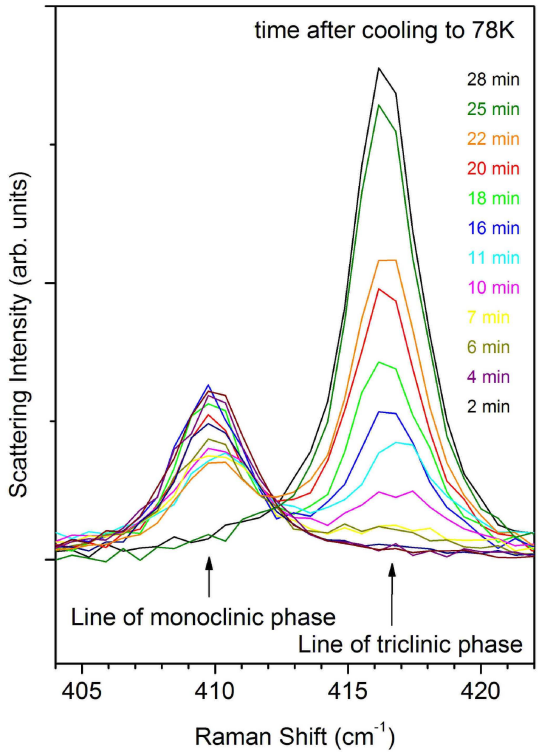

FIG. 7: (Color online) Time-dependent Raman scattering spectra of $Nb_2O_2F_3$ as the sample was cooled from 100 K to 78 K and kept at this temperature. Gradual development of the triclinic phase is obvious.

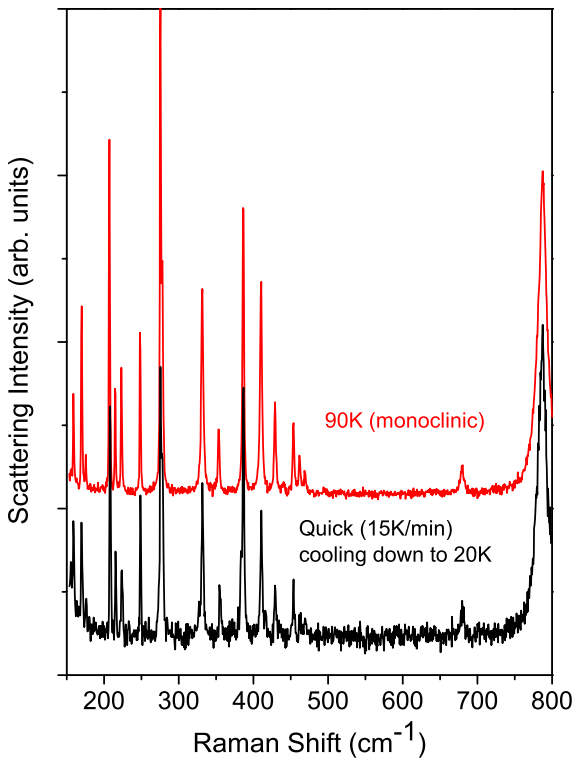

FIG. 8: (Color online) Raman scattering spectra of $Nb_2O_2F_3$ in its high-temperature monoclinic phase at T=90 K (red curve) and quickly cooled sample to T=20 K (black curve). Obvious is a persistence of the monoclinic phase at low temperature. Lower signal-to-noise ratio for the T=20 K spectrum is due to short accumulation time.

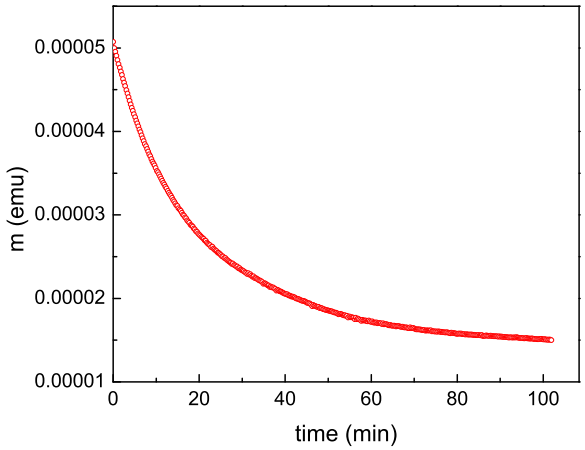

FIG. 9: (Color online) Time relaxation of the magnetization (m) after sample cooling from 100 K to 75 K and fixing the temperature. The decrease of m is due to the slow transformation from the monoclinic to the triclinic phase.

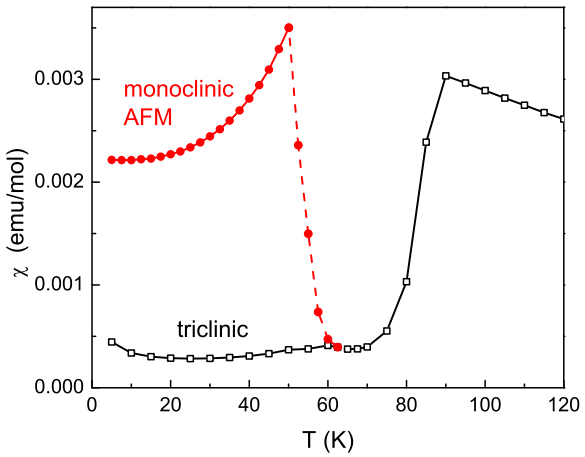

FIG. 10: (Color online) Magnetic susceptibility in the triclinic (circles) and quenched monoclinic (open squares) phases measured upon warming. The dashed line indicates the transition from monoclinic to triclinic phase.

clearly observes two non-overlapping lines, corresponding to the high-temperature monoclinic (at 410 cm^{-1}) and the low-temperature triclinic (at 416 cm^{-1}) phase. It is seen that initially the monoclinic line dominates the scattering spectrum. However, after 6-8 minutes the line of the triclinic phase appears in the spectra, which signals the development of corresponding crystallographic phase. Simultaneously the volume fraction of the monoclinic phase starts to decrease, as the intensity at 410 cm^{-1} line diminishes. Only after about 25-30 min one observes predominant contribution of the triclinic phase.

Identical experiments with sample cooling from 100 K to lower temperatures (70 K and 60 K) show similar, but faster kinetics of the transition, when the monoclinic-triclinic transformation appears to be completed within only several minutes.

Another striking effect is observed upon fast (15 K/min) cooling of the sample. In this case, as it is shown in Fig. 8, quick cooling of the sample to as low as 20 K results in "bypassing" the structural monoclinic-to-triclinic transformation so that the monoclinic phase remains the dominant crystallographic phase of the sample even at low temperatures. Careful analysis of Raman line intensities shows, however, some minor contribution from the low-temperature triclinic phase, even though the volume fraction of this latter is estimated to be only at the level of 5%.

In order to confirm and support the conclusions from Raman measurements we have conducted a time-dependent magnetization study. Fig. 9 shows magnetization data acquired after fast sample cooling from 100 K to 75 K, i.e. just below the structural phase transition temperature. After stabilizing temperature at 75 K, the magnetization of $Nb_2O_2F_3$ continues to decrease as a function of time for more than 1 hour. This time dependence is a consequence of rather slow transformation from the monoclinic to the triclinic phase. While the monoclinic phase is paramagnetic with relatively high magnetic suscepti-

bility, the triclinic phase has low magnetic susceptibility due to the pairing of the two electrons (spins) on one of the two Nb-Nb dimers within the unit cell in a spin singlet state.[1–3] Therefore, a decrease of magnetization in Fig. 9 reflects a slow kinetics of the structural transformation, consistent with the Raman data of Fig. 7.

In order to achieve the thermodynamic equilibrium and nearly complete transformation of the monoclinic phase into the triclinic one, the temperature change through the structural transition has to be extremely slow. In Fig. 10 we display with open squares the magnetic susceptibility of $Nb_2O_2F_3$ measured upon warming after waiting for several hours in the temperature range below 90 K. The susceptibility below the structural transition is small and shows only minor temperature dependence, which is consistent with a spin singlet state of the two electrons forming a bond on every other Nb-Nb dimer. Faster cooling, however, results in a significantly larger low temperature susceptibility and a stronger temperature dependence, as shown in Fig. 10 (bold red circles, measured after fast quenching to 5 K). It is obvious that the quenched monoclinic phase shows a sharp phase transition at T_N=49 K, which is characterized by a distinct decrease of the magnetic susceptibility towards lower temperature. This behavior is typical for a phase with antiferromagnetic order and, therefore, it can be concluded that the single spins (per dimer) of the quenched monoclinic phase order antiferromagnetically below T_N. This is also consistent with the high temperature susceptibility of $Nb_2O_2F_3$, which follows a Curie-Weiss law with a negative Weiss temperature.[1] Upon increasing temperature beyond 50 K the quenched monoclinic phase becomes unstable and converts into more stable triclinic phase, as indicated by the dashed line in Fig. 10, before it transforms back into the high temperature monoclinic structure at $T_c = 90$ K.

Conclusions

In summary, the lattice vibrational spectra of a reduced niobium oxyfluoride crystals, $Nb_2O_2F_3$, are studied experimentally by Raman scattering and theoretically within DFT lattice dynamics calculations. Experimentally observed lines are assigned to the specific lattice eigenmodes in the high-temperature monoclinic phase a well as low-temperature triclinic phases. Vibrations of Nb-Nb dimers are found to possess frequencies as high as 382 cm^{-1}.

A non-trivial dynamics of the crystallographic monoclinic-to-triclinic phase transition is observed: fast sample cooling to low temperatures results in preservation of high-temperature crystallographic phase even at 20 K. On the other hand, cooling sample to slightly below T_c and keeping the temperature fixed allows to observe rather slow (up to 30-60 min.) dynamics of the structural phase transition. This slow kinetics is confirmed by time dependent magnetization measurements. The magnetic properties of both structures at low temperature are determined in long time annealing (triclinic phase) and fast quenching (monoclinic phase) experiments. The data suggest a possible antiferromagnetic order below $T_N \approx$ 49 K in the quenched monoclinic phase.

Acknowledgements

This work was supported in part by the R. A. Welch Foundation (E-1297), the State of Texas through the Texas Center for Superconductivity, and the US AFOSR.

[1] T. Thao Tran, M. Gooch, B. Lorenz, A. P. Litvinchuk, M. G. Sorolla II, J. Brgoch, P. C. W. Chu, and A. M. Guloy, J. Am. Chem. Soc. **137**, 636 (2015).
[2] S. V. Streltsov and D. I. Khomskii, Proc. Nat. Acad. Sci. **113**, 10491 (2016);
[3] V. V. Gapontsev, D. I. Khomskii, and S. V. Streltsov, J. Magn. Magn. Mater. **420**, 28 (2016);
[4] D. M. Korotin, V. I. Anisimov, and S. V. Streltsov, Sci. Reports **6**, 25831 (2016).
[5] S. V. Streltsov and D. I. Khomskii, Phys. Rev. B **86**, 064429 (2012).
[6] G. Kliche and H. G. von Schnering, Z. Naturforsch. B **44**, 74 (1989).
[7] W. Preetz, K. Harder, H. G. von Schnering, G. Kliche, and K. Peters, J. Alloys Compnd. **183**, 413 (1992).
[8] N. T. Lucas, J. P. Blitz, S. Petrie, R. Stranger, M. G. Humphrey, G. A. Heath, and V. Otieno-Alego, J. Am. Chem. Soc. **124**, 5139 (2002).
[9] J. P. Perdew, K. Burke, and M. Ernzerhof, Phys. Rev. Lett. **77**, 3865 (1996).
[10] S. J. Clark, M. D. Segall, C. J. Pickard, P. J. Hasnip, M. J. Probert, K. Z. Refson, and M. C. Payne, Z. Kristallogr. **220**, 567 (2005).
[11] H. J. Monkhorst and J. D. Pack, Phys. Rev. B **13**, 5188 (1976).
[12] D. L. Rousseau, R. P. Bauman, and S. P. S. Porto, J. Raman Spectr. **10**, 253 (1983).
[13] I. P. Ipatova, A. A. Maradudin, and R. F. Wallis, Phys. Rev. **155**, 882 (1967).
[14] M. Balkanski, R. F. Wallis, and E. Haro, Phys. Rev. B **28**, 1928 (1983).
[15] A. P. Litvinchuk, M. N. Iliev, V. N. Popov, and M. M. Gospodinov, J. Phys.: Cond. Matter **16**, 809 (2004);
[16] J. Laverdiere, S. Jandl, A. A. Mukhin, V. Yu. Ivanov, V. G. Ivanov, and M. N. Iliev, Phys. Rev. B **73**, 214301 (2006).
[17] M. N. Iliev, A. P. Litvinchuk, H.-G. Lee, C. L. Chen, L. M. Dezaneti, C. W. Chu, V. G. Ivanov, M. V. Abrashev, and V. N. Popov, Phys. Rev. B **59**, 364 (1999).
[18] J. F. Scott, R. C. C. Leite, and T. C. Damen, Phys. Rev. **188**, 1285 (1969).
[19] M. Ya. Valakh, A. P. Litvinchuk, G. S. Pekar, and G. N. Polisskii, Phys. Status Solidi B **104**, 743 (1981).
[20] M. Ya. Valakh and A. P. Litvinchuk, Fiz. Tverd. Tela **27**, 1958 (1985).
[21] M. V. Abrashev, A. P. Litvinchuk, C. Thomsen, and V. N. Popov, Phys. Rev. B **55**, R8638 (1997).
[22] M. Ya. Valakh, A. P. Litvinchuk, V. M. Dzha-

gan, V. O. Yukhymchuk, Ye. O. Havryliuk, M. Guc, I. V. Bodnar, V. Izquierdo-Rocca, A. Pérez-Rodríguez, and D. R. T. Zahn, RSC Adv. **6**, 67756 (2016).